Materials Transactions, Vol. 45, No. 7 (2004) pp. 2224 to 2231
Special Issue on Ultrafine Grained Structures

Effect of Deformation Temperature and Strain Rate on Evolution of Ultrafine Grained Structure through Single-Pass Large-Strain Warm Deformation in a Low Carbon Steel

Akio Ohmori[1,*1], Shiro Torizuka[1], Kotobu Nagai[1], Naoshi Koseki[2,*2] and Yasuo Kogo[2]

[1]*National Institute for Materials Science, Tsukuba 305-0047, Japan*
[2]*Department of Material Science and Technology, Faculty of Industrial Science and Technology, Tokyo University of Science, Noda 278-8510, Japan*

Ultrafine grained structure formed dynamically through a severe warm deformation in the temperature range from 773 K to 923 K has been investigated in a 0.16%C-0.4%Si-1.4%Mn steel. The effects of the deformation conditions such as deformation temperature and strain rate on microstructural evolution were examined using a single-pass compression technique with a pair of anvils. A large plastic strain up to 4 was imposed on the specimen interior at a strain rate of 1 or 0.01 s^{-1}. Ultrafine ferrite grains surrounded by high angle boundaries, whose nominal grain size ranged from 0.26 to 1.1 μm, evolved when the equivalent plastic strain exceeded the critical value about 0.5 to 1, and increased with an increase in strain without any large-scale migration of high angle boundaries. The effects of deformation conditions on microstructural evolution of ultrafine grained structures can be summarized into the Zener-Hollomon(Z-H) parameter dependences. The average size and the volume fraction of newly evolved ultrafine grains depend on the Z-H parameter. Decreasing Z-H parameter enhances the formation of equiaxed ultrafine grains. These indicate that the mechanism forming ultrafine grained structures through the warm severe deformation in the present study is similar to "continuous recrystallization" or "*in-situ* recrystallization" and that some activation process during or after the deformation plays an important role in the microstructural evolution.

(Received March 17, 2004; Accepted May 11, 2004)

Keywords: *low carbon steel, severe deformation, warm deformation, ultrafine grain, ferrite, microstructure, large strain, Zener-Hollomon parameter, grain size, misorientation*

1. Introduction

Grain refinement in metallic materials brings a dramatic increase in yield strength and remarkable improvement in toughness simultaneously without any costly alloying. In the manufacturing process of steels, the TMCP (Thermo-Mechanical Controlled Processing) has undergone development as a grain refinement technique that can achieve a marked improvement in performance and high productivity at the same time. Therefore TMCP has been put to very wide use.

Recently, many studies on ultrafine grained microstructures whose grain sizes are smaller than about 1 μm have been performed to develop new ecologically beneficial high-performance steels. Several novel techniques to obtain ultrafine grained low-alloyed ferritic steels have been proposed there.[1)] They can be classified roughly into two types of thermo-mechanical processes. One is the process where an ultrafine grained ferrite structure is formed through the phase transformation from austenite to ferrite during or after severe plastic deformations imposed on austenite.[2–4)] It may be interpreted as a pursuit of a further development of the conventional TMCP.

The other is the process where an ultrafine grained ferrite structure is directly formed out of a deformed ferrite structure through a severe cold or warm plastic deformation without any phase transformation. Bulky steels with ultrafine grained structures of submicrons to several tens of nanometers have been fabricated by the process containing various intense straining techniques, such as mechanical milling,[5,6)] equal channel angular pressing/extrusion (ECAP/ECAE),[7,8)] cyclic extrusion compression (CEC),[9)] accumulative roll-bonding (ARB),[10,11)] multi-axial and multiple compressions,[12,13)] caliber-rolling[14–16)] etc.

In the recent studies,[12,13,17)] the formation process of an ultrafine grained structure through a severe cold or warm deformation has often been recognized to be different from the classic recrystallization, namely discontinuous recrystallization that is well-known microstructural evolution process in which a new grain structure is formed from a deformed structure. Discontinuous recrystallization is understood as the two-stage process composed of nucleation and growth of recrystallized grains surrounded by high-angle boundaries, while the formation process of an ultrafine grained structure through a severe cold or warm deformation is considered as the one-stage process, as it were, comprising only nucleation without any large scale migration of grain boundaries.

Therefore, in order to describe such phenomenon compared with discontinuous recrystallization, terminologies as follows have been proposed: continuous recrystallization,[12,13,18)] *in-situ* recrystallization,[17)] geometric recrystallization,[19)] rotation recrystallization,[20)] extended recovery,[21)] and so on. There are still many unclear points in the details of each definition and mechanism of the phenomenon described by these terminologies.

In order to utilize the above-mentioned phenomena related to recrystallization for practical grain refinement techniques, it is necessary to clarify the details of the microstructural evolution systematically. The authors *et al.*[22,23)] have applied a technique of compression with a pare of anvils to introduce a large strain up to 4 (in true strain) into the interior of a steel specimen by a single-pass warm deformation while controlling the deformation conditions, namely, deformation tem-

*[1]Present address: Steel Research Laboratory, JFE steel Co., Kurashiki 712-8511, Japan
*[2]Graduate Student, Tokyo University of Science

perature and strain rate. This technique is more suitable for basic systematic experiments for studying the essence of the phenomena as compared with the other intense straining techniques above-mentioned because it can eliminate the effect of complex strain caused by multi-pass or multi-axial deformations.

The authors[24] have already revealed that the Zener-Hollomon parameter,[25] which is representative of a deformation condition, governs the mean grain size of ultrafine grained ferrite newly evolved through severe warm deformations. In the present study, we note the amount of the newly evolved high-angle boundaries and ultrafine grains. The effects of deformation conditions such as deformation temperature, strain rate, strain, on the microstructural evolution of ultrafine grained ferrite structures through single-pass warm deformations were investigated using the technique of a compression with anvils for a low carbon steel. Formation of new boundaries and ultrafine grains were determined quantitatively.

2. Experimental Procedure

A commercial JIS SM490 grade hot-rolled steel plate with a chemical composition of 0.16%C-0.4%Si-1.4%Mn (mass%) was used in this study. Its detailed chemical composition is shown in Table 1. Test specimens having dimensions of 15 long × 13 wide × 12 thick (mm) were cut from the steel plate. The initial microstructure was a lamellar structure in which ferrite and pearlite bands stratified alternatively as shown in Fig. 1. The nominal ferrite grain size was 15 μm and the average intervals of pearlite bands was 27 μm.

The specimens were heated to a temperature of 773 K, 823 K or 873 K below the A_{c1} temperature, which is about 993 K, using a thermo-mechanical heat treatment simulator capable of controlling their temperature and the deformation

Table 1 Chemical composition of the steel (mass%).

C	Si	Mn	P	S
0.16	0.41	1.43	0.014	0.004

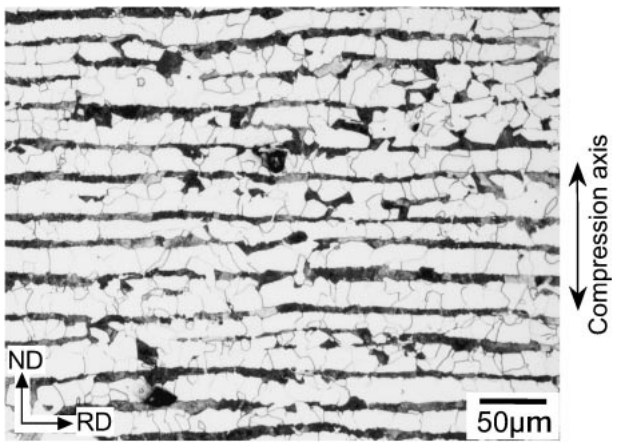

Fig. 1 Optical micrograph of the initial microstructure of the steel.

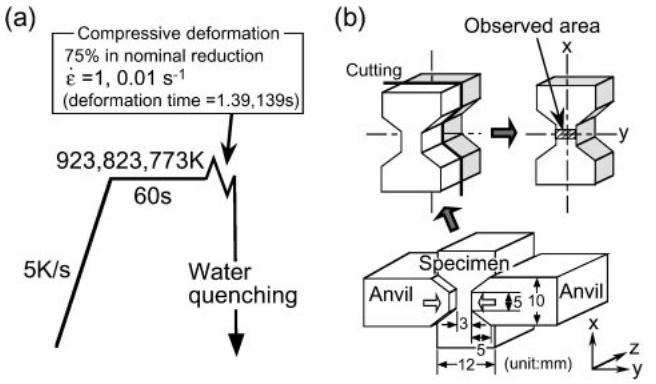

Fig. 2 Schematic illustrations showing (a) the conditions of heat treatment and deformation, and (b) the compression by a pair of anvils.

conditions. Their temperatures were measured by thermocouples welded on the surface at the thickness center of each specimen. After holding for 60 s at the elevated temperature, they were compressed by 75% in nominal reduction, from 12 mm to 3 mm in thickness, with a pair of anvils. And then they were quenched immediately from the deformation temperatures. Figure 2 illustrates the anvil compression test in the present study.

The compressive deformations were carried in the time periods of 1.39 s and 139 s so as to obtain the apparent nominal strain rates $\dot{\varepsilon}$ of $1\,s^{-1}$ and $0.01\,s^{-1}$, respectively. Compression axis was perpendicular to the pearlite bands of the initial microstructure.

After cutting and polishing, the specimens were etched in 1.5% nital, and the microstructures on the cross section as indicated in Fig. 2(b) were observed under an optical microscope and a SEM.

Furthermore, in order to measure the misorientation of grain boundaries, EBSP (Electron Backscattering Pattern) analyses were carried out with a Schottky-type FE-SEM (Philips XL30 SFEG). The OIM™ (Orientation Imaging Micrograph™) system of TexSEM Lab. Inc. was used in data analyses. Densities of grain boundaries, namely boundary length in unit area observed, and nominal grain sizes of newly evolved ultrafine ferrite were examined by analyzing the boundary images obtained by EBSP analysis. Nominal grain size was defined by the square root of the average grain area in the present study.

3. Results

3.1 Strain distribution in interior of specimen

In the anvil compression test adopted in this study, strain concentrates at the center of a specimen and forms a continuous distribution across in the interior of a specimen.[23] Local compressive strain introduced in each part of the specimen can be estimated from a change in interval of the pearlite bands before and after deformation. Because the present observed area is almost under a plane strain condition,[26] a local equivalent plastic strain ε_{eq} can be found by eq. (1)

$$\varepsilon_{eq} = \frac{2}{\sqrt{3}} \ln\left(\frac{l_0}{l}\right) \tag{1}$$

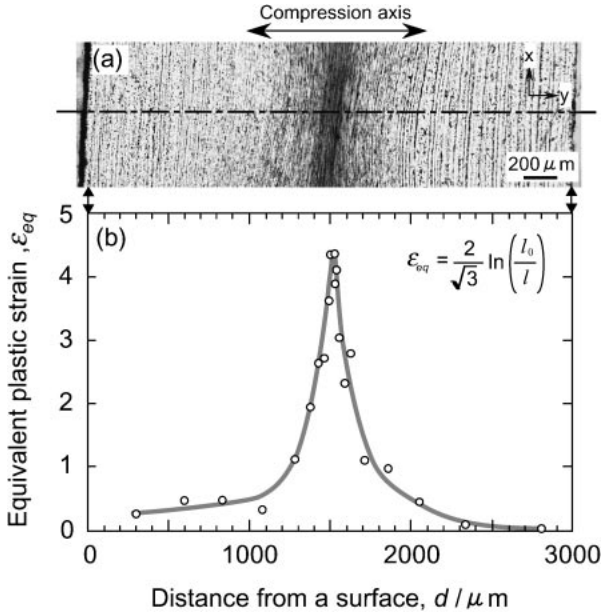

Fig. 3 (a) Optical micrograph of the specimen deformed at 773 K and a strain rate of 1 s^{-1}, and (b) distribution of equivalent plastic strain through thickness.

where l_0 is the initial interval of pearlite bands before the deformation and l is that after the deformation.

An optical micrograph through the thickness of a specimen deformed at 773 K and a nominal strain rate of 1 s^{-1} is shown in Fig. 3(a). The intervals of the pearlite bands become narrower as it gets closer to the center from the surface of the specimen and it is apparent that strain concentrates at the center. Fig. 3(b) shows the distribution of the equivalent plastic strains estimated by eq. (1) where l is the average intervals for every 10 pearlite bands. Equivalent plastic strain is distributed in the range of 0 to about 4. Similar distributions were found for the specimens deformed under other conditions. These experimental results are in agreement with the results of FE-analyses.[22,26)]

Using the strain distribution in the interior of a specimen after the anvil compression test, it is possible to observe a change in microstructure with an increase in strain in one specimen.

3.2 Change in microstructure with strain

Figures 4 and 5 show the changes in microstructure with an increase in strain. The former shows the SEM micrographs and the boundary maps obtained by EBSP analysis for a specimen deformed at 923 K and a nominal strain rate of 0.01 s^{-1}, and the latter shows those at 773 K and the same strain rate. In the boundary maps, the grain boundaries are distinguished by using three colors according to the misorientation angle, θ. The red line expresses high angle boundaries of $\theta \geqq 15^\circ$. The dark blue and light blue lines express low angle boundaries of $5^\circ \leqq \theta < 15^\circ$ and $1.5^\circ \leqq \theta < 5^\circ$ respectively. The black point indicates the invalid data where the image quality(IQ) or the confidence index(CI) is too low ($IQ < 50$ or $CI < 0.1$). The image quality represents the clearness of Kikuch diffraction pattern, and the confidence index represents the reliability of a determination of crystal orientation.

Examples of the image quality maps by EBSP analysis are

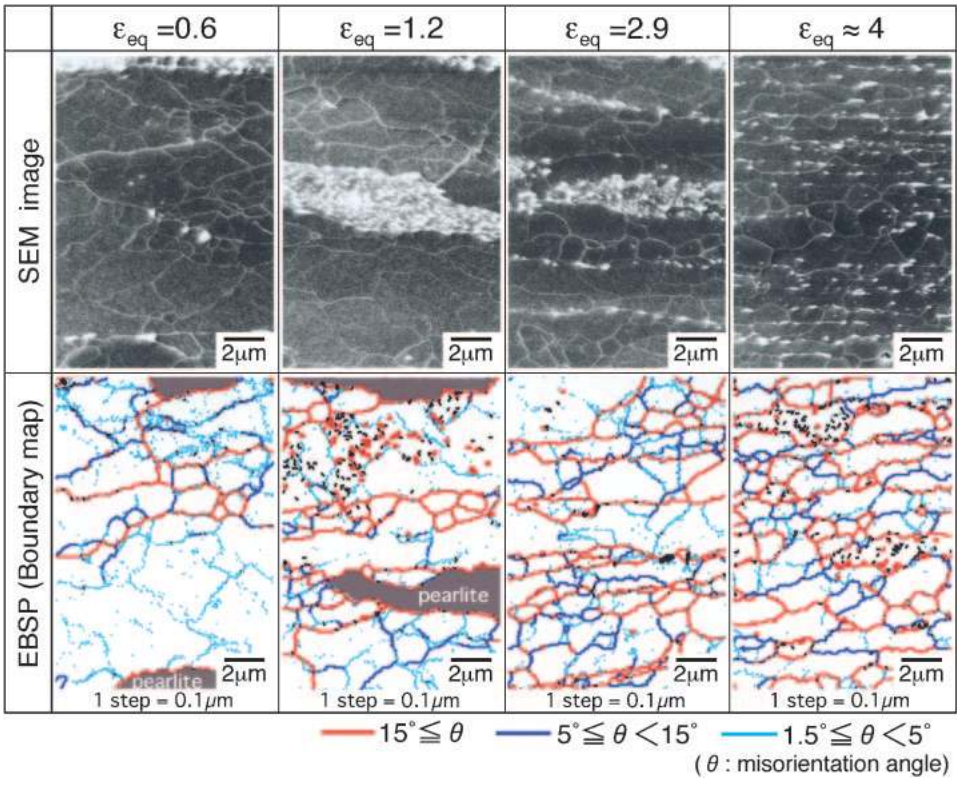

Fig. 4 SEM micrographs and boundary maps obtained by EBSP analysis showing change in microstructure with strain for the specimen deformed at 923 K and a nominal strain rate of 0.01 s^{-1}.

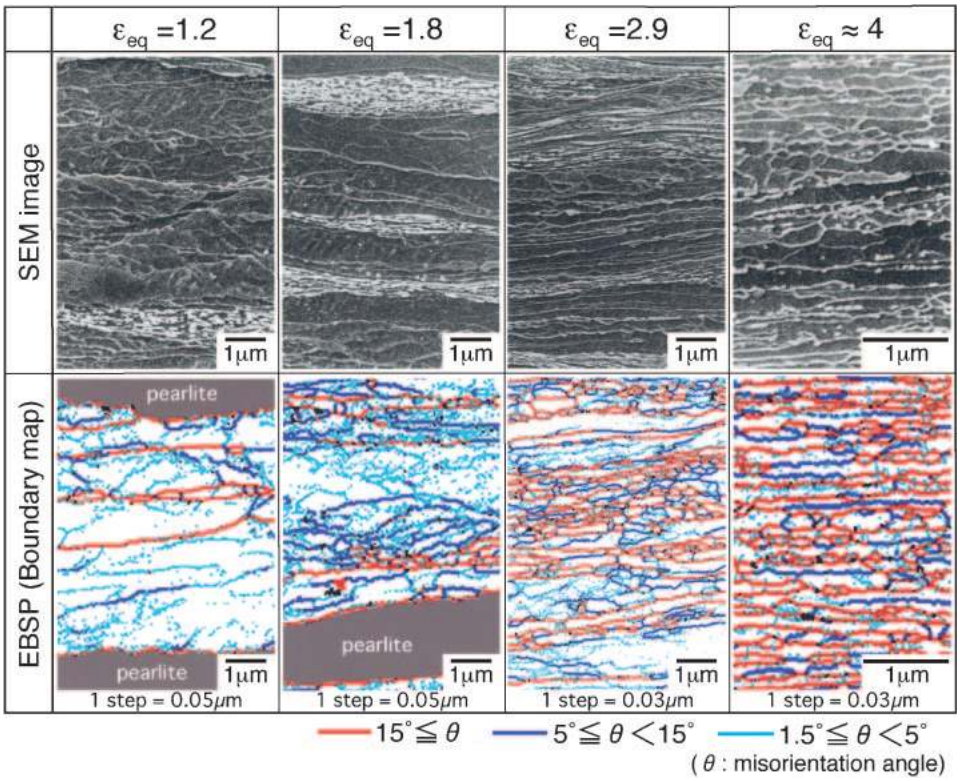

Fig. 5 SEM micrographs and boundary maps obtained by EBSP analysis showing change in microstructure with strain for the specimen deformed at 773 K and a nominal strain rate of 0.01 s^{-1}.

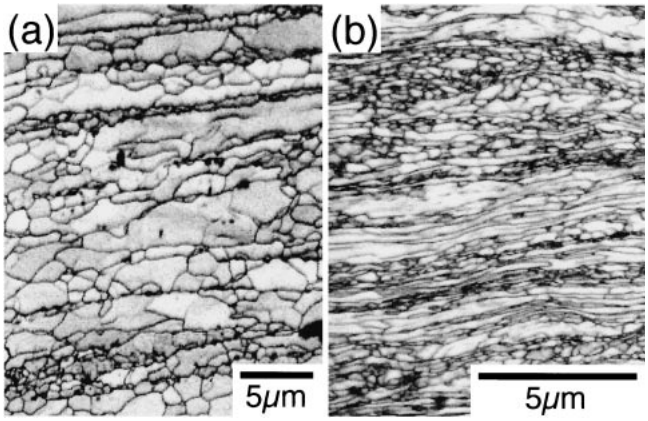

Fig. 6 Image quality maps where $\varepsilon_{eq} = 2.9$ with a strain rate of 0.01 s^{-1} and a deformation temperature of (a) 923 K or (b) 773 K.

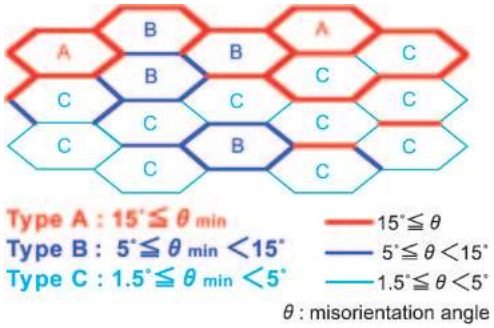

Fig. 7 Classification of grains according to the misorientation.

shown in Fig. 6 for the same specimens shown in Fig. 4 and Fig. 5. The clear contrast between the boundary and the grain interior is an evidence that the dislocation density was not so high in the interior of the grains even under a large strain of 2.9. This indicates that the dislocation density in the interior of newly evolved grains or subgrains decrease due to some dynamic restoration process and that a clear grain boundary structure is built.

In either case of Fig. 4 and Fig. 5, high angle boundaries increased with an increase in strain. Ultrafine ferrite grains surrounded by the high angle boundaries were newly generated especially along the initial grain boundaries and the interfaces between pearlite and ferrite, and they increased in number with an increase in strain. Pearlite was segmented and transformed into the rows of spheroidized cementite particles. The ultrafine grained structures containing newly evolved equiaxed ferrite grains were obtained in the area of the maximum equivalent strain over 4. Those observations indicate that the formation of the ultrafine grains is a process of fragmentation or subdivision of initial grains by the strain-induced high angle boundaries. Large-scale migration of high angle boundaries was not observed in the process.

As compared Fig. 4 and Fig. 5, the effect of the deformation temperature on microstructural evolution is revealed. Critical strain required to generate the ultrafine grains surrounded by the newly evolved high angle boundaries increased from about 0.5 to 1 with an increase in deformation temperature. The area fraction and the average size of the ultrafine grains decreased with a decrease in deformation temperature.

In order to clarify the changes in microstructure with strain under various deformation conditions, the grain boundaries

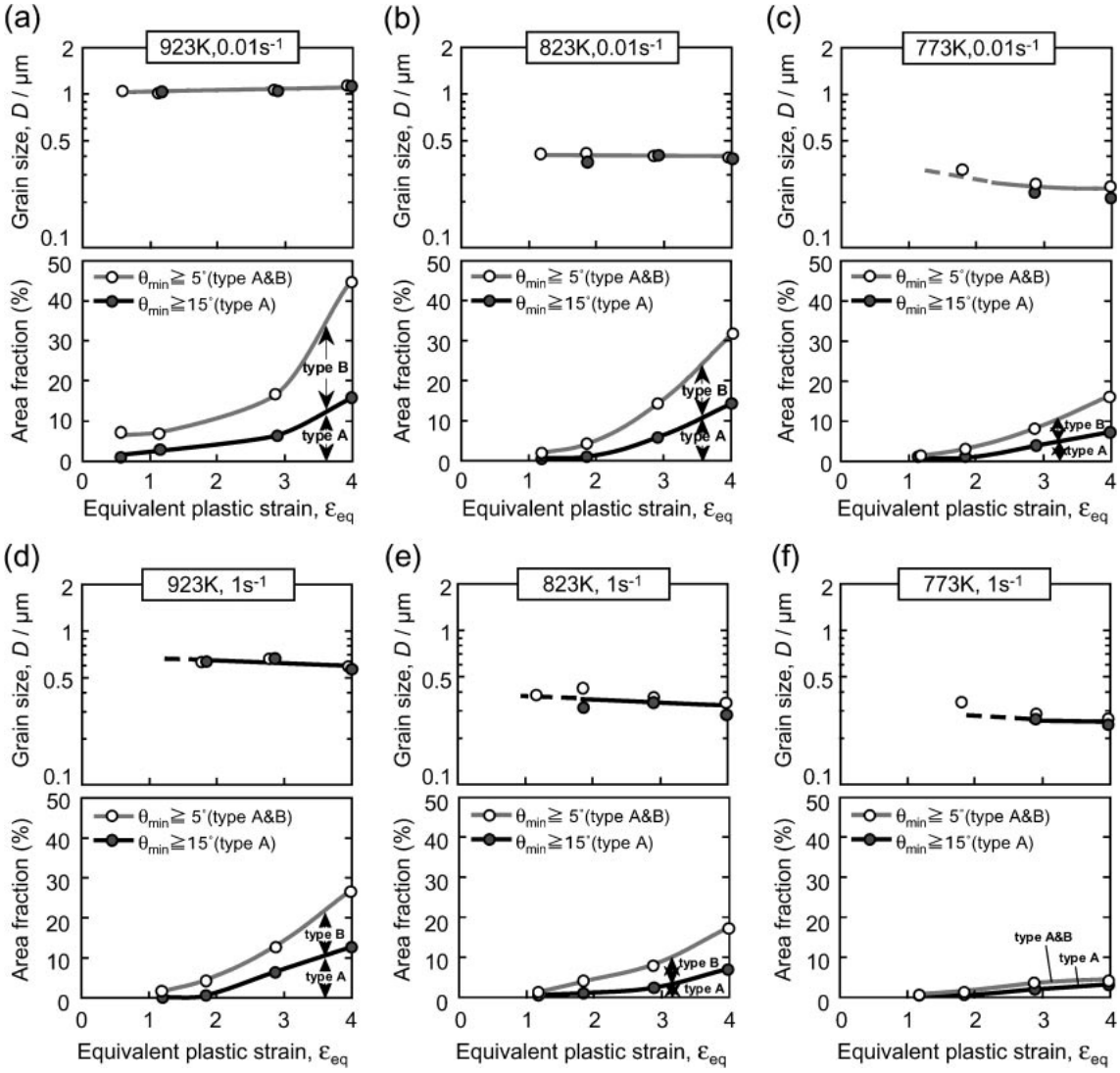

Fig. 8 Change in the average grain size and the area fraction of newly evolved grains surrounded by boundaries having misorientation larger than 15° or 5° under various deformation temperatures and nominal strain rates of (a) 923 K, 0.01 s^{-1}, (b) 823 K, 0.01 s^{-1}, (c) 773 K, 0.01 s^{-1}, (d) 923 K, 1 s^{-1}, (e) 823 K, 1 s^{-1}, and (f) 773 K, 1 s^{-1}.

(including sub-boundaries) were classified into three types according to the misorientation and were quantified respectively. Moreover, the newly evolved grains (including subgrains) were classified into three types as shown in Fig. 7, according to the minimum misorientation of the boundaries surrounding each grain.

Figure 8 shows the change in the area(volume) fraction and the average size of newly evolved ferrite grains surrounded by the boundaries having a misorientation larger than 15° (grains of type A) or 5° (grains of type A&B) with strain under various deformation conditions. The average grain sizes ranged from 0.26 to 1.1 μm. The grain size did not depend on strain for all the deformation conditions, while the area fraction of the newly evolved grains increased monotonically with an increase in strain. They were already in steady sizes although the microstructural changes were still in progress in the strain range up to 4.

Figure 9 shows the change in length fraction and density (boundary length per unit observed area of 1 μm^2) of each classified type of boundary under various deformation conditions. The length fraction and the density of high angle boundaries having a misorientation larger than 15° monotonically increased with an increase in strain, while the length fraction of sub-boundaries having a misorientation smaller than 5° decreased. This indicates that the average misorientation of all the boundaries increases with increasing strain.

The effects of deformation conditions are discussed next.

4. Discussions

4.1 Controlling factor of newly evolved grain size

It is generally known that the grain size formed through discontinuous dynamic recrystallization in a steady state deformation is governed by the Zener-Hollomon parameter (Z-H parameter),[25] which is expressed by $Z = \dot{\varepsilon} \exp(Q/RT)$ where $\dot{\varepsilon}$ is the strain rate (s^{-1}), R is the gas constant (8.314 J/mol·K), Q is the apparent activation energy of deformation (J/mol) and T is the deformation temperature (K). The authors[24] have previously revealed that the average grain

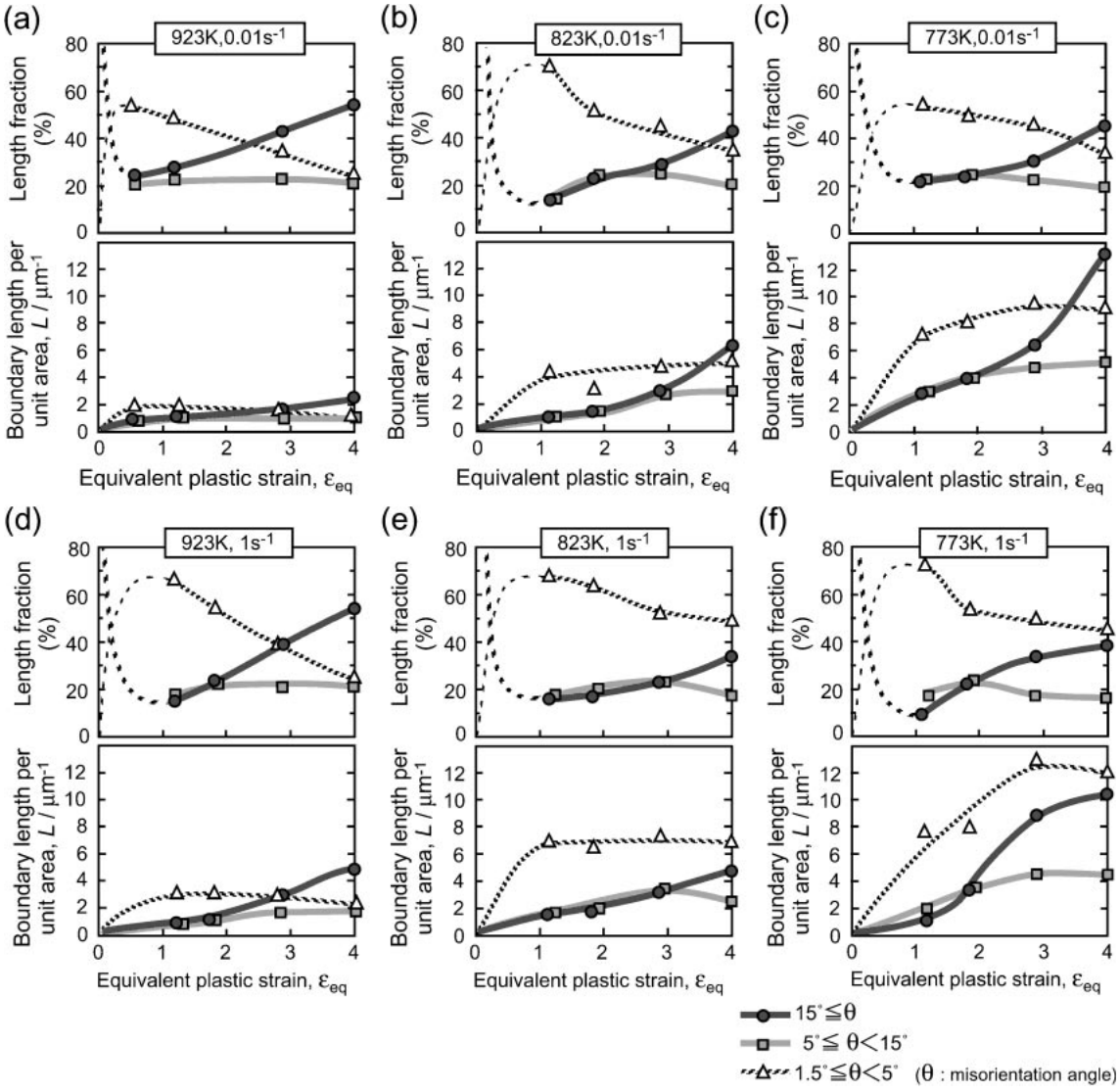

Fig. 9 Change in the length fraction and the density of boundaries classified into three types according to misorientation under various deformation temperatures and nominal strain rates of (a) 923 K, 0.01 s^{-1}, (b) 823 K, 0.01 s^{-1}, (c) 773 K, 0.01 s^{-1}, (d) 923 K, 1 s^{-1}, (e) 823 K, 1 s^{-1}, and (f) 773 K, 1 s^{-1}.

size of the ultrafine grained structure formed through the warm compressive deformations is governed by the Z-H parameter.

In the present study, the average size of newly evolved grains surrounded by boundaries having misorientation larger than 5° is almost steady under a large imposed strain of about 4 as shown in Fig. 8. Accordingly, the Z-H parameter dependency of the steady state grain size can be illustrated as shown in Fig. 10. The activation energy of self-diffusion in ferromagnetic ferrite iron, which is 254 kJ/mol,[27] was used as Q for estimating Z-H parameter.

In case of a higher strain rate of 1 s^{-1}, heat generation caused by the severe deformation cannot be neglected. The rises in temperature by 12 K, 31 K and 39 K were observed during the deformations at 923 K, 823 K and 773 K respectively. Therefore the peak temperature during a deformation was used as the deformation temperature.

The data on IF(interstitial free) steel reported by Tsuji *et al.*[28] were also plotted together in Fig. 10 in order to compare the size of grains formed by a discontinuous dynamic recrystallization (DRX) with that formed through a severe warm deformation in our studies. The data in our studies are on a single straight line and the relationship expressed by $D(\mu m) = 10^{1.97}Z^{-0.162}$ is established between the average grain size D and the Z-H parameter.

It is noted that they are on an extrapolated line of the data on subgrains reported by Tsuji *et al.* rather than that on recrystallized grains formed through discontinuous dynamic recrystallization (DRX). This indicates that the size of newly evolved ultrafine grains surrounded by high angle boundaries is almost equal to that of sub-structures, such as subgrains and dislocation cells, formed dynamically through the deformations in the present study. Therefore large-scale migration of high angle boundaries does not occur in the microstructural evolution process through the severe warm deformation, while it occurs in the process of discontinuous recrystallization which consists of two stages of nucleation and growth. It is considered that the evolution of an ultrafine grained structure is formed through dynamic and static recovery of a deformed structure. Such process can be

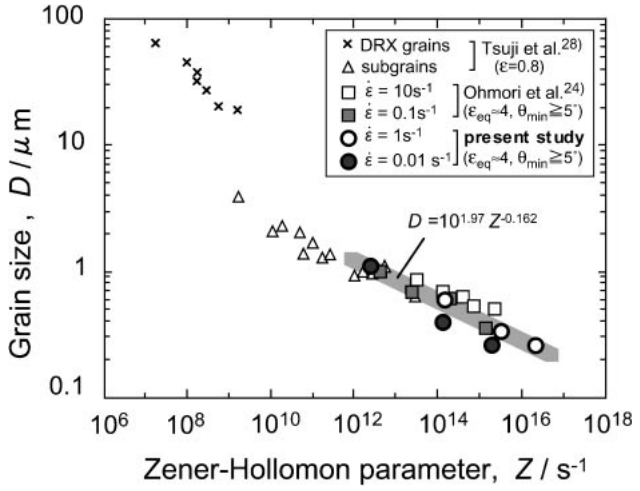

Fig. 10 Z-H parameter dependency of the average size of newly evolved grains surrounded by the boundaries having misorientation larger than 5°.

understood to be similar to the microstructural evolution mechanism called "continuous recrystallization" or "*in-situ* recrystallization".

4.2 Effects of Z-H parameter on evolution of ultrafine grained structure

The effects of the deformation conditions such as strain rate or deformation temperature on the evolution of ultrafine grains were experimentally revealed as shown in Fig. 9. They can be rearranged by using the Z-H parameter as shown in Fig. 11. The area fraction of newly evolved grains surrounded by the boundaries with misorientation larger than 15° (grains of type A) or 5° (grains of type A&B) decreases with an increase in the Z-H parameter. The formation of ultrafine grains is enhanced by a decrease in the Z-H parameter, that is an increase in deformation temperature or a decrease in strain rate. This indicates that some activation process plays an important role in the formation process of the ultrafine grains.

On the other hand, the formation of strain-induced high angle boundaries shows a different tendency. Figure 12 shows the effects of the Z-H parameter on the length fraction and the density (boundary length per unit area of 1 μm^2) of high angle boundaries. The density of high angle boundaries increases with an increase in the Z-H parameter although the scatter in the data seems large. The effect of the deformation conditions on the length fraction is relatively small. These tendencies indicate that the formation of strain-induced high angle boundaries increases with an increase in the Z-H parameter in contrast to the formation of the grains.

The fact that the Z-H parameter determines the microstructural evolution reveals that the foundation of an ultrafine grained structure is formed dynamically and that the process is closely related to thermal activation process during and after the deformation.

The microstructural evolution process is schematically illustrated in Fig. 13. This is simply based on the concept of "continuous recrystallization" or "*in-situ* recrystallization". Strain-induced local misorientation resulting in a newly evolved high angle boundary increases with an increase in strain (Fig. 13(a)→(b)→(c)). More straining develops lamellar dislocation walls or boundaries perpendicular to

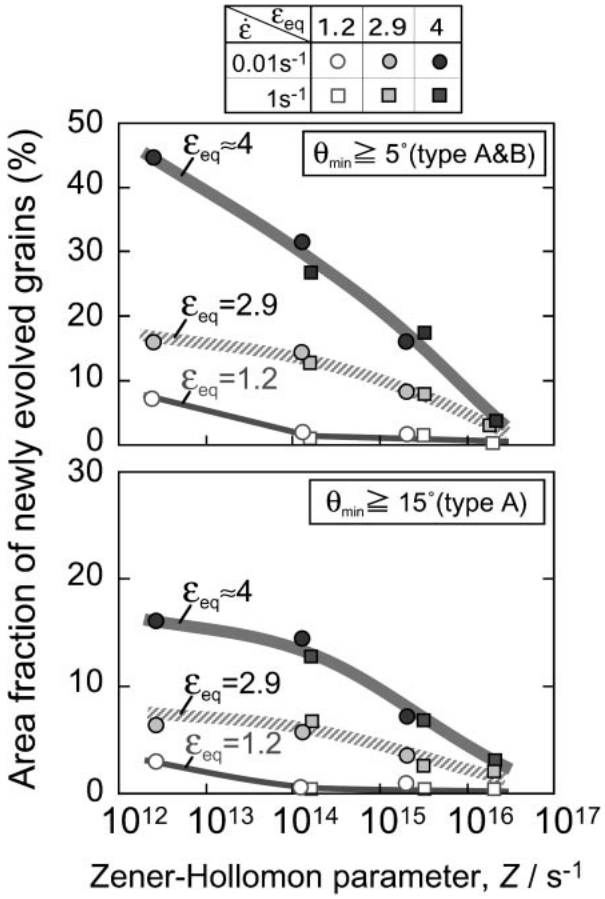

Fig. 11 Effects of Z-H parameter on the area fraction of newly evolved ferrite grains.

the compressive axis (Fig. 13(c)). Hughes and Hansen[29] have demonstrated such grain subdivision mechanisms accompanied by the formation of lamellar boundaries in case of fcc metals.

Thermal activation processes such as recovery, small-scale migration of boundaries *etc.* enhance the rearrangement of the boundaries, and assist the formation of equiaxed ultrafine grains or subgrains (Figs. 13(e), (f), (g)). Increasing the Z-H parameter suppresses the thermal activation process and keeps the lamellar boundaries which do not contribute to forming equiaxed grains.

5. Conclusions

Ultrafine grained structures formed dynamically through single-pass warm compressive deformations at elevated temperatures under A_{c1} were investigated in a 0.16%C-0.4%Si-1.4%Mn. The following conclusions were obtained.

(1) The formation process of an ultrafine grained ferrite structure is similar to that called continuous recrystallization or *in-situ* recrystallization.

(2) The average size of newly evolved ultrafine grains surrounded by high angle boundaries is governed by the Z-H parameter. It decreases with an increase in the Z-H parameter.

(3) The formation of ultrafine grains is enhanced by a decrease in the Z-H parameter, while the formation of strain-induced high angle boundaries increases with an

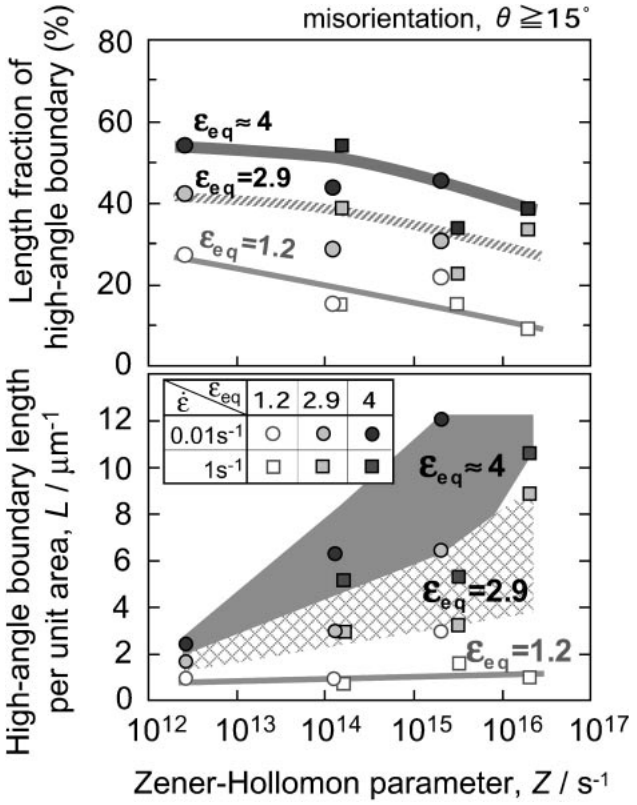

Fig. 12 Effects of Z-H parameter on the length fraction and the density of high angle boundaries.

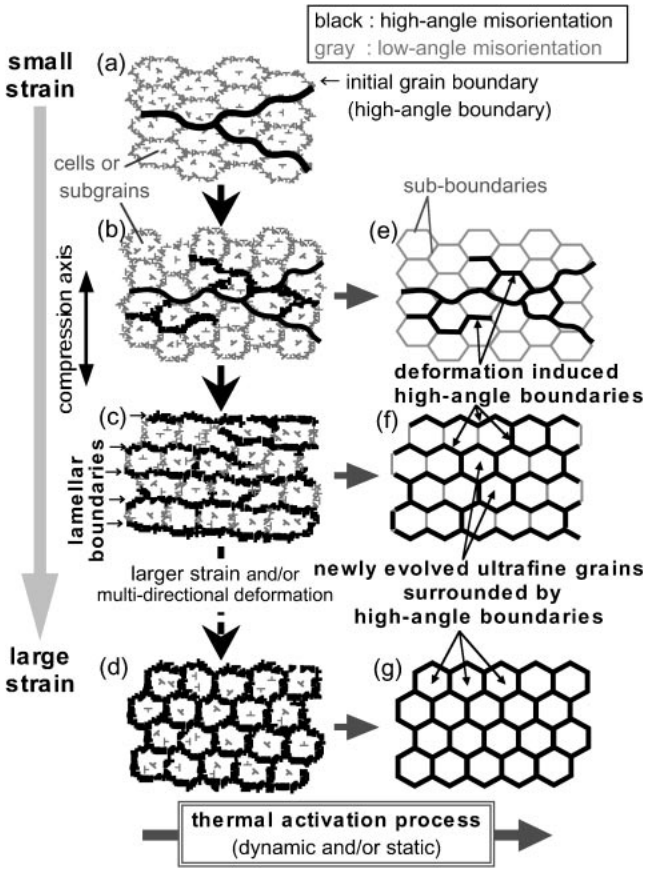

Fig. 13 Schematic illustration showing the forming process of ultrafine-grained structures through the warm severe deformations.

increase in the Z-H parameter within the range of deformation conditions in the present study.

(4) Thermal activation processes are considered important for forming an equiaxed ultrafine grained structure in this microstructural evolution process.

REFERENCES

1) M. Niikura, Y. Hagiwara, K. Nagai, K. Tsuzaki and S. Takaki: Proc. of Int. Symp. on Ultrafine Grained Steels, (The Iron and Steel Inst. of Japan, 2001) pp. 26–33.
2) P. J. Hurley and P. F. Hodgson: Mater. Sci. Tech. **17** (2001) 1360–1368.
3) J. K. Choi, D. H. Seo, J. S. Lee, K. K. Um and W. Y. Choo: ISIJ Int. **43** (2003) 746–754.
4) S. Torizuka and K. Nagai: Mater. Sci. Forum **426–432** (2003) 4573–4578.
5) Y. Kimura and S. Takaki: Mater. Trans., JIM **36** (1995) 289–296.
6) J. Yin, M. Umemoto, Z. G. Liu and K. Tsuchiya: ISIJ Int. **41** (2001) 1389–1396.
7) A. Azushima, K. Aoki and T. Inoue: Tetsu-to-Hagane **84** (1998) 762–766 (in Japanese).
8) D. H. Shin, J. J. Park, S. Y. Chang, Y. K. Lee and K. T. Park: ISIJ Int. **42** (2002) 1490–1496.
9) M. Richert, Q. Liu and N. Hansen: Mater. Sci. Eng. **A260** (1999) 275–283.
10) N. Tsuji, Y. Saito, H. Utsunomiya and S. Tanigawa: Scr. Mater. **40** (1999) 795–800.
11) Y. Saito, H. Utsunomiya, N. Tsuji and T. Sakai: Acta Mater. **47** (1999) 579–583.
12) A. Belyakov, T. Sakai, H. Miura and R. Kaibyshev: ISIJ Int. **39** (1999) 592–599.
13) A. Belyakov, T. Sakai and H. Miura: Mater. Trans., JIM **41** (2000) 476–484.
14) K. Nagai: J. Mater. Process Technol. **117** (2001) 329–332.
15) F. Yin, T. Hanamura, O. Umezawa and K. Nagai: Mater. Sci. Eng. **A354** (2003) 31–39.
16) A. Ohmori, S. Torizuka, K. Nagai, N. Koseki and Y. Kogo: Tetsu-to-Hagane **89** (2003) 781–788 (in Japanese).
17) N. Tsuji, R. Ueji, Y. Ito and Y. Saito: Proc. of 21st RISØ Int. Symp. on Materials Science (RISØ National Laboratory, Denmark, 2000) pp. 105–112.
18) A. Belyakov, T. Sakai, H. Miura, R. Kaibyshev and K. Tsuzaki: Acta Mater. **50** (2002) 1547–1557.
19) M. E. Kassner, H. J. McQueen and E. Evangelista: Mater. Sci. Forum **113–115** (1993) 151–156.
20) M. R. Druby and F. J. Humphreys: Acta Metall. **34** (1986) 2259–2271.
21) F. J. Humphreys and M. Hatherly: *Recrystallization and Related Annealing Phenomena*, (Elsevier Science Ltd., Oxford, 1995) pp. 167 and 377.
22) I. Salvatori, T. Inoue and K. Nagai: ISIJ Int. **42** (2002) 744–750.
23) D. W. Suh, S. Torizuka, A. Ohmori, T. Inoue and K. Nagai: ISIJ Int. **42** (2002) 432–439.
24) A. Ohmori, S. Torizuka, K. Nagai, K. Yamada and Y. Kogo: Tetsu-to-Hagane **88** (2002) 857–864 (in Japanese).
25) C. Zener and J. H. Hollomon: Trans. ASM **33** (1945) 955–965.
26) T. Inoue, S. Torizuka, K. Nagai, K. Tsuzaki and T. Ohashi: Mater. Sci. Technol. **17** (2001) 1580–1588.
27) D. W. James and G. M. Leak: Philos. Mag. **14** (1966) 701–713.
28) N. Tsuji, Y. Matsubara, Y. Saito and T. Maki: J. Japan Inst. Metals. **62** (1998) 967–976.
29) D. A. Hughes and N. Hansen: Acta Mater. **45** (1997) 3871–3886.